



**HAL**  
open science

# Type-constrained robust fitting of quadrics with application to the 3D morphological characterization of saddle-shaped articular surfaces

Stéphane Allaire, Jean-José Jacq, Valérie Burdin, Christian Roux, Christine Couture

## ► To cite this version:

Stéphane Allaire, Jean-José Jacq, Valérie Burdin, Christian Roux, Christine Couture. Type-constrained robust fitting of quadrics with application to the 3D morphological characterization of saddle-shaped articular surfaces. MMBIA'07: IEEE 8th Computer Society Workshop on Mathematical Methods in Biomedical Image Analysis 11th IEEE International Conference on Computer Vision (ICCV'07), Oct 2007, Rio De Janeiro, Brazil. pp.1 - 8, 10.1109/ICCV.2007.4409163 . hal-02164443

**HAL Id: hal-02164443**

**<https://hal.science/hal-02164443>**

Submitted on 25 Jun 2019

**HAL** is a multi-disciplinary open access archive for the deposit and dissemination of scientific research documents, whether they are published or not. The documents may come from teaching and research institutions in France or abroad, or from public or private research centers.

L'archive ouverte pluridisciplinaire **HAL**, est destinée au dépôt et à la diffusion de documents scientifiques de niveau recherche, publiés ou non, émanant des établissements d'enseignement et de recherche français ou étrangers, des laboratoires publics ou privés.

# Type-Constrained Robust Fitting of Quadrics with Application to the 3D Morphological Characterization of Saddle-Shaped Articular Surfaces

Stéphane Allaire  
Princess Margaret Hospital  
Radiation Medicine Program  
Toronto ON M5G 2M9, Canada  
allaire.stephane@gmail.com

Jean-José Jacq, Valérie Burdin,  
Christian Roux, GET-ENST Bretagne  
& INSERM U650, Labo. de Traitement de  
l'Information Médicale 29200 Brest, France  
<http://latim.univ-brest.fr/>

Christine Couture  
Laboratoire d'Anthropologie  
des Populations du Passé CNRS  
UMR 5199, Université Bordeaux 1  
33405 Talence cedex, France

## Abstract

*The scope of this paper is the guaranteed fitting of specified types of quadratic surfaces to scattered 3D point clouds. Since we chose quadrics to account for articular surfaces of various shapes in medical images, the models thus estimated usefully extract global symmetry-related intrinsic features in human joints: centers, axes, extremal curvatures. The unified type-enforcing method is based on a constrained weighted least-squares minimization of algebraic residuals which uses a robust and bias-corrected metric. Provided that at most one quadratic constraint is involved, every step produces closed-form eigenvector solutions. In this framework, guaranteeing the occurrence of 3D primitives of certain types among this eigendecomposition is not a straightforward transcription of the priorly handled 2D case. To explore possibilities, we re-exploit a mapping to a 2D space called the Quadric Shape Map (QSM) where the influence of any constraint on shape and type can in fact be studied visually. As a result, we provide a new enforceable quadratic constraint that practically ensures types such as hyperboloids, which helps characterize saddle-like articular surfaces. Application to a database shows how this guarantee is needed to coherently extract the center and axes of the ankle joint.*

## 1. Context of characterization with prior

Previous works on the characterization of articular bone surfaces have focused mostly on *local* features. They have followed a piecewise patch approach, using various sorts of free-form surfaces, such as the popular approximation B-splines [1]. Along with Finite-Element Models, these continuous parametrical representations aim to accurately and finely reproduce bone surfaces, without restraining or modeling in terms of shape. In contrast, our purpose is to extract significant *overall symmetries* in 3D articular surfaces. Given that these surfaces first grew coherently during morphogenesis and get smoothed daily by a person's repeated motions, the extracted intrinsic reference frame may give us additional meaningful insight into the functionality that is made possible in a joint. We

therefore follow a *model-driven* approach. Our choice of *quadrics* as models is primarily motivated by their two important strengths. First, such algebraic surfaces meet our desire for *global* characterization. Secondly, the second-order information that they magnify provides us with *prime symmetries*. Such a model is deliberately reductive with respect to anatomical surfaces. Nevertheless, the *generic* implicit quadratic model is rich, since it subdivides into various types of primitives, which can be relevant to given articular surfaces. For instance, in the hip ball-and-socket joint, an ellipsoid –possibly a sphere– is used to support the analysis of a necrotic femoral head, as exemplified in [2], whereas in the elbow hinge joint, the humeral trochlea may be best characterized by a hyperboloid of one sheet.

Besides, published works performing *algebraic surface fitting* mostly address applications in computer vision, pattern recognition or reverse engineering [3, 4, 5, 6, 7, 8, 9, 10]. They deal with 3D manufactured industrial objects and the feature to be retrieved within the acquired data is in most cases their *exact* designed shape. When relying on 2D images, it becomes appropriate to *specifically* extract ellipses and lines, for instance, since they are perspective projections of cylindrical, circular and straight parts of the objects [7, 8, 5, 6, and reviews therein]. If 3D samples are available, direct explicit registration with the known shape model will usually be preferred (pose estimation). In contrast, the objects we wish to characterize are bone surfaces involved in skeletal joints. They result from natural anatomical shaping, which fulfills adaptation in particular at the scale of species, which evolve in their environment, and individuals, who grow from embryos, work and practice sport in their surroundings, who get old and also recover from traumas or orthopedic surgery. Thus, there is *no ground truth* for a suitable quadric primitive, but only possible knowledge-based expectations about its relevant type. Though conceptually the context is different from usual applications, we share a common background of estimation methodology. As pointed out, a 3D fitting scheme is in particular required in the field of application to *natural shape characterization*. An accumulator-based approach is then impracticable due to the parameter space dimension. Instead, *minimizing* an

objective function using robust techniques is appropriate. However, the current challenge is about moving on to 3D in regards to *constraining a specified type*.

In this paper, we investigate possibilities to *guarantee* specified types, even when it may seem irrelevant, due to: a) the occurrence of pathological or degraded structures, while a repeatable characterization and comparable results are needed; or b) our desire to provide experts with an option that would incorporate their knowledge.

Throughout the literature, we can delineate several approaches to obtain the expected type of quadratic curve or surface. Generic non-typologically constrained quadric fitting might be successful, provided the data shape is already close enough to a quadric of the expected type. Yet, in our case, the initial shape may not allow a good model match. Choosing among output eigen-solutions [4, 2], taking advantage of the deformation bias induced by the normalization factor [5], or using curvature weights [6], may help. Nevertheless all of these techniques provide *no guarantee* about the type of quadric; neither do iterative methods with rejection testing following parameter nudging [11] or data point selection [5]. The tuning of a specialized parameterization for each particular type of quadric [9, 10] can provide some guarantee. However, this implies the loss of the closed-form linearity at each step; moreover, it lacks practical genericity. The only way to keep to direct resolution is to rely on algebraic constraints, through investigating extensions of the innovation that A.W. Fitzgibbon, M. Pilu and R.B. Fisher made in the mid-nineties to guarantee an ellipse at fitting conic curves to any input 2D data [7]. To our knowledge, so far only the ellipsoid type has been addressed in this way [12, 13].

Recently, we have revisited the ellipsoid-specific constraint lately provided by Q. Li and J.G. Griffiths [12] as a robustly enforceable ellipsoid-guarantee [13]. To this end, we have exploited the bi-dimensional diagram called the *Quadric Shape Map* (QSM) which we had previously introduced with the distinct purpose of analyzing and comparing the output primitives of a fitting procedure [2]. Here, we propose to re-exploit this meaningful representation for a comprehensive exploration of all constraint possibilities, which justifies a new typological guarantee.

Note that the model through the intermediary of which we extract features is simple. Consequently, the expectable local discrepancies, potentially exaggerated by the added constraining, must be handled during the fitting process by *robust* methods which possibly reject some *outliers* [2, 8, 13]. Furthermore, as regards data, usual errors are to occur while they are acquired, preprocessed and segmented. The input point cloud may be sparse and unevenly scattered.

The outline of this paper is as follows. In section §2, we provide a synthetic description of the constrained robust fitting process, as our chosen methodological framework.

In section §3, we provide helpful mathematical tools: geometric invariants and the Quadric Shape Map which we briefly present as a visualization tool from our new perspective. On this basis, we recall how to identify the type of a fitted quadric without ambiguity. And in section §4, the QSM lets us explore in detail how to practically guarantee that a specified type of quadric is output through a chosen quadratic constraint in the fitting process. This leads us to derive and study a new constraint which is specific to types of quadrics that have at least one hyperbolic section, such as hyperboloids. In section §5 we apply it to available anthropological ankle samples, not to lessen the full relevance of our method to *medically involved saddle-like surfaces*. Lastly we conclude with a discussion.

## 2. Methodology for constrained robust quadric fitting

We use a transcription to the case of quadric surfaces in 3D, like in [13], of the unified constrained least-square framework earlier introduced for 2D conic fitting by [7, 8].

### 2.1. Minimization problem statement

An *exact quadric surface* is defined implicitly in the 3D space as the zero-level set of a second-order polynomial:

$$f : \mathbf{x}(x, y, z) \mapsto f(\mathbf{a}, \mathbf{x}) = \mathbf{a}^T \boldsymbol{\chi}, \quad (1)$$

with the *parameter vector*  $\mathbf{a}$  and the *basis vector*  $\boldsymbol{\chi}$ :

$$\mathbf{a} = [a_{xx} \ a_{yy} \ a_{zz} \ a_{yz} \ a_{zx} \ a_{xy} \ a_x \ a_y \ a_z \ a_1]^T; \quad (2)$$

$$\boldsymbol{\chi} = [x^2 \ y^2 \ z^2 \ yz \ zx \ xy \ x \ y \ z \ 1]^T. \quad (3)$$

For a given cloud of  $n$  data points  $p_i = [x_i \ y_i \ z_i]^T$  and the associated *regression vectors*  $\boldsymbol{\chi}_i$ , the estimate of  $\mathbf{a}$  is sought for, that defines the most globally relevant quadric with derived axes, center and semi-axes, and a revealed type.

In what follows, our methodological choices: a) of the metric considered, b) of the kind of constraint enforced and c) of the core estimation technique, are all related. They are driven by our main objectives: 1) simplicity (respect of the genericity of the model, no computational complexity); 2) option of typological guarantee to incorporate prior knowledge; 3) robustness to the expected local inadequacies, be they inherent of the global and constrained model or/and due to upstream errors in the analysis workflow; 4) semi-interactive scenario (few intuitive parameters, intuitive displayable outputs).

To be able to use a closed-form linear method, we take the squares of the residuals  $f(\mathbf{a}, p_i)$  as straightforward measures of errors. Yet we use a robust redescending M-estimator (Tukey's biweight [8]) and correct the first order of the bias induced by not using the Euclidean distances [2]. The implied nonlinear minimization is carried out by a classical Iterative Reweighted Least-Square (IRLS) process, via successive linear steps. Each step minimizes the residual  $\chi^2$ , where the weighted scatter matrix  $\mathcal{S}_w$  with

weights  $w_i^{(j-1)}$  has got updated from the previous iteration:

$$\chi^2 = \sum_{i=1}^n w_i^{(j-1)} f(\mathbf{a}, \mathbf{p}_i)^2 = \mathbf{a}^T \left[ \sum_{i=1}^n w_i^{(j-1)} \boldsymbol{\chi}_i \boldsymbol{\chi}_i^T \right] \mathbf{a} = \mathbf{a}^T \mathbf{S}_w \mathbf{a}. \quad (4)$$

## 2.2. Properties of enforceable constraints

At each fitting step, even when no typological constraint is required on the output, it is necessary to scale the parameter vector by a normalization factor in order to avoid the trivial zero solution  $\mathbf{a} = \mathbf{0}_{10}$ . Provided *at most one quadratic* constraint is enforced, a linear direct closed-form resolution is possible, as described next in §2.3. It is expressed via a non homogeneous equality with a symmetric *constraint matrix*  $\mathbf{C}$  and a non-zero scalar constant  $c$ :

$$\mathbf{a}^T \mathbf{C} \mathbf{a} = c, \text{ with } \mathbf{C} = \begin{pmatrix} \mathbf{C}_q & \mathbf{0}_{6 \times 4} \\ \mathbf{0}_{4 \times 6} & \mathbf{0}_{4 \times 4} \end{pmatrix}. \quad (5)$$

Profitably, such a constraint a) is invariant under orientation-preserving isometries of the data and proportional to coordinate scaling since it only involves the coefficients related to the quadric *shape* in  $f$  (see §3.1); b) can be given a typological meaning. In the generic case without prior knowledge, the normalizing constraint ideally bears no singularities among quadrics [3, 2]. In contrast, a *specific* constraint attempts to be discriminating among types of quadrics; how we choose the specific nonsingular  $6 \times 6$  submatrix  $\mathbf{C}_q$  and constant  $c$  is in §4.2.

## 2.3. Eigenvector-based core estimation technique

With a Lagrange multiplier  $\lambda$ , the Lagrangian reads:

$$L(\mathbf{a}, \lambda) = \mathbf{a}^T \mathbf{S}_w \mathbf{a} + \lambda (c - \mathbf{a}^T \mathbf{C} \mathbf{a}). \quad (6)$$

At each linear fitting step, the first-order optimality necessary condition on the Lagrangian (6) reads:

$$\mathbf{S}_w \mathbf{a} = \lambda \mathbf{C} \mathbf{a}. \quad (7)$$

Thus a minimizer  $(\lambda, \mathbf{a})$  must be an eigenvalue–eigenvector solution of the generalized eigenvalue problem (7). In addition, we can simply derive the residual chi-square (4):

$$\chi^2 = \mathbf{a}^T \mathbf{S}_w \mathbf{a} = \lambda c. \quad (8)$$

Using Sylvester’s Law of inertia, A.W.Fitzgibbon, M.Pilu and R.B.Fisher showed that the generalized eigenvalues of the problem (7) have exactly the same signs as the eigenvalues of the constraint matrix  $\mathbf{C}$ , up to permutation [7]. Consequently, the weighted least-square solution minimizing (4) subject to the quadratic constraint (5) is the eigenvector  $\mathbf{a}$  of the problem (7) associated with the eigenvalue  $\lambda$  that is simultaneously: a) the sign of  $c$  (or equivalently such that  $\mathbf{a}^T \mathbf{C} \mathbf{a}$  is the sign of  $c$  in (5) [8]); and b) closest to zero in absolute value to minimize the residual  $\chi^2$  (8). Yet, our bone shape characterization scheme allows the anatomy expert to discard that, and *interactively* choose the relevant primitive among the 6 eigen outputs.

## 3. Distinguishing types of quadrics

### 3.1. Tools to build and understand constraints

The functional (1) defining a quadric may be expressed as an *affine quadratic form*:

$$f: \mathbf{x} \mapsto f(\mathbf{a}, \mathbf{x}) = \mathbf{x}^T \boldsymbol{\Omega} \mathbf{x} + \mathbf{l}^T \mathbf{x} + k, \quad (9)$$

where the symmetric block matrix  $\boldsymbol{\Omega}^h$  represents the corresponding homogeneous quadratic form:

$$\boldsymbol{\Omega}^h = \begin{bmatrix} \boldsymbol{\Omega} & \frac{\mathbf{l}}{2} \\ \frac{\mathbf{l}^T}{2} & k \end{bmatrix} = \begin{bmatrix} a_{xx} & \frac{a_{xy}}{2} & \frac{a_{zx}}{2} & \frac{a_x}{2} \\ \frac{a_{xy}}{2} & a_{yy} & \frac{a_{yz}}{2} & \frac{a_y}{2} \\ \frac{a_{zx}}{2} & \frac{a_{yz}}{2} & a_{zz} & \frac{a_z}{2} \\ \frac{a_x}{2} & \frac{a_y}{2} & \frac{a_z}{2} & a_1 \end{bmatrix}. \quad (10)$$

It can be shown easily that both the homogeneous quadratic form and the quadratic form  $\mathbf{x} \mapsto \mathbf{x}^T \boldsymbol{\Omega} \mathbf{x}$  will not be affected by orientation-preserving similarities on the quadric, namely rotations, translations, and scalings, unlike both the linear form  $\mathbf{x} \mapsto \mathbf{l}^T \mathbf{x}$  and the constant form  $\mathbf{x} \mapsto k$ . As a consequence, the former two quadratic forms are *uniquely attached* to the quadric considered, which can therefore be classified among different types according to their algebraic characteristics.

The eigen decomposition of the symmetric matrix  $\boldsymbol{\Omega}$  yields its –all real– eigenvalues  $\alpha_i$  that define the shape of the quadric, and its eigenvectors which are the three orthogonal axes of the quadric. The coefficients of the characteristic polynomial of  $\boldsymbol{\Omega}$  are combinations of these eigenvalues and are therefore invariant under changes of direct orthonormal bases. With respect to  $\boldsymbol{\Omega}$ , they are namely its trace, the sum denoted  $\sum \det^p_2(\boldsymbol{\Omega})$  of its three principal second-order minors, and its determinant:

$$\begin{aligned} \alpha_1 + \alpha_2 + \alpha_3 &= \text{tr}(\boldsymbol{\Omega}) = a_{xx} + a_{yy} + a_{zz} \\ \sum_{i \neq j} \alpha_i \alpha_j &= \sum \det^p_2(\boldsymbol{\Omega}) = \begin{vmatrix} a_{yy} & \frac{a_{yz}}{2} \\ \frac{a_{yz}}{2} & a_{zz} \end{vmatrix} + \begin{vmatrix} a_{zz} & \frac{a_{zx}}{2} \\ \frac{a_{zx}}{2} & a_{xx} \end{vmatrix} + \begin{vmatrix} a_{xx} & \frac{a_{xy}}{2} \\ \frac{a_{xy}}{2} & a_{yy} \end{vmatrix} \\ \alpha_1 \alpha_2 \alpha_3 &= \det(\boldsymbol{\Omega}). \end{aligned} \quad (11)$$

In summary, we have an invariant of every order with respect to the parameter vector  $\mathbf{a}$ : the first is linear, the second is quadratic, and the third is cubic. They make up a generating basis for all *symmetric* polynomials of order up to three in the eigenvalues  $\alpha_i$  of  $\boldsymbol{\Omega}$ . Let us also consider the base-independent quartic determinant of the homogeneous quadratic form in (10):  $\det(\boldsymbol{\Omega}^h)$ . As well as helping output type identification (§3.2), these invariants help us build specific input constraints (§4), since in this last case one cannot distinguish the role played by each eigenvalue of  $\boldsymbol{\Omega}$ .

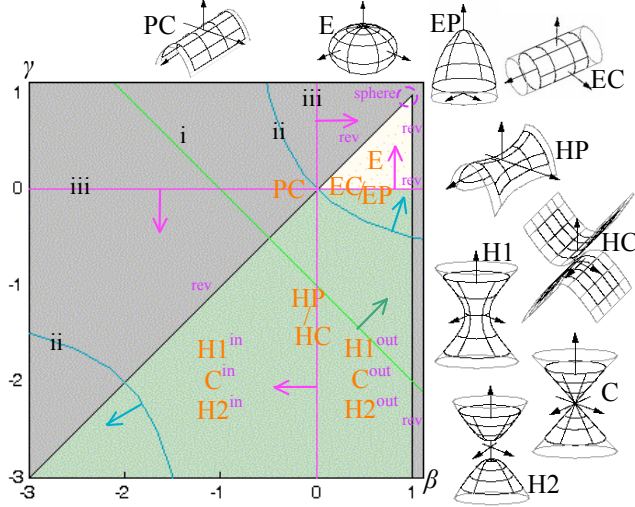


Figure 1: Plots in the QSM (12, 13, Table 1) [2] of the oriented zero-level sets of the 3 basal invariants (11): i. the trace, ii. the sum of second-order minors, and iii. the determinant, of the matrix  $\Omega$  representing the quadratic form attached to every quadric

In order to search for enforceable constraints based on such quantities and study their influence, we re-exploit the bi-dimensional diagram called the *Quadric Shape Map* (QSM) which was introduced originally for mensuration analysis of output primitives [2]. As reproduced in the background of Fig.1, this 2D layout locates characteristic zones for the useful types of quadrics, and also spots peculiar shapes such as ones of revolution (see Table 1). The QSM helpfully allows interpretation in terms of *shape continuity* and *typological transitions*, yet it is not to be read linearly. The two coordinate axes ( $\beta, \gamma$ ) express the relative ratios of two eigenvalues with respect to the numerically highest third one for every considered 3D quadric. The QSM is based on mere unrestrictive conventions with respect to the eigenvalues of  $\Omega$ :

$$\alpha_1 \geq \alpha_2 \geq \alpha_3 \quad \text{and} \quad \alpha_1 > 0. \quad (12)$$

The ratios are further defined as follows:

$$\alpha_2 = \beta \alpha_1 \quad \text{and} \quad \alpha_3 = \gamma \alpha_1, \quad \text{with} \quad 1 \geq \beta \geq \gamma. \quad (13)$$

For the purpose of constraint studying only, note that, contrary to [2], the quadric surface normal vectors are not outward-pointing by convention. The lower left quadrant is thus exceptionally not grayed out in Fig.1 (nor in Fig.2).

Each point in the QSM carries the information of the type and anisotropy of the associated quadrics, which is

E	Ellipsoid
H1, H2, C	Hyperboloid of 1 sheet, of 2 sheets, Cone
EP, HP	Elliptic, Hyperbolic Paraboloid
EC, HC, PC	Elliptic, Hyperbolic, Parabolic Cylinder

Table 1: Abbreviations for the useful types of quadrics. In addition, <sup>rev</sup> advises a quadric is of revolution around some axis; <sup>out</sup> and <sup>in</sup> show whether normals are outward- or inward-pointing

now ideal for designing constraints *regardless of pose and scale*. It is actually both a quantitative and intuitive representation that is very analogous in significance to the 1D *continuous* scale of eccentricity for 2D conics. Given any function of the eigenvalues of  $\Omega$ , we can assess its specificity with respect to one or a few types of quadrics by plotting in the QSM its zero-level set or its sign map. For instance, Fig.1 displays the invariants listed in §3.1. It gets clear that the sign of  $\text{tr}(\Omega)$  is *not a reliable criterion* when classifying types of quadrics (see §3.2), whereas the sign of  $\det(\Omega)$  does match the discriminating boundaries between groups of types. However, if each type needs to be identified, then  $\Omega^h$  must further be taken into account.

### 3.2. Identifying each type of quadric

Out of the 17 types in the classification of quadrics [14], in Table 2 we focus only on the 9 types of quadrics that may be reliable primitives of extraction. This is useful for identifying the particular type of a quadric corresponding to any parameter vector  $\mathbf{a}$  output by the fitting algorithm.

*Remark.* As a notion, the *inside* of a quadric surface is naturally defined as lying within the convexity of each sheet. Now, mathematically, the normals of the surface are given by the gradient of the functional (9). These can thus be either *outward-pointing* (<sup>out</sup>) or *inward-pointing* (<sup>in</sup>). Parameter vector  $-\mathbf{a}$  defines the same quadric in terms of implicit zero set as  $\mathbf{a}$  does, yet with opposite surface orientation. The point is that, not only this changes the sign of  $\text{tr}(\Omega)$ , but also the sign of the cubic determinant: in 3D,  $\det(-\Omega) = -\det(\Omega)$ . Thus to account for the quadric surface orientation, we define the flag  $v$  as a unit root which equals  $-1$  if the normals are inward-pointing and  $+1$  otherwise.

### 4. Enforcing specified types of quadrics

Now we focus on *guaranteeing* the type of quadric at each closed-form fitting step of the iterated process.

In the 2D case of conic sections, proper conic types can be discriminated according to the sign of  $\det(\Omega)$ , which is a quadratic quantity. A. Fitzgibbon *et al.* had the idea of merging such an inequality constraint with the needed normalization factor [7]. By enforcing  $4\det(\Omega)=+1$ , they made sure that an ellipse would be obtained [7]. Similarly, hyperbolas can be found in any data by enforcing  $4\det(\Omega)=-1$ . (Let us point out that this also allows pairs of

	$\det(\Omega^h) < 0$	$\det(\Omega^h) > 0$	$\det(\Omega^h) = 0$
$\det(v\Omega) > 0$	E	–	(single point)
$\det(v\Omega) < 0$	H2	H1	C
$\det(\Omega) = 0$	EP	HP	EC, HC, PC (or degenerated)

Table 2: Classification of the real types of quadrics (Table 1) according to the determinants of affine and homogenous quadratic forms (13, 10), and the normals-orientation flag  $v$  (see §3.2)

secant lines, which are likely to be found, unlike the zero-radius ellipse.) Both cases are expressed by involving the same  $3 \times 3$  constraint submatrix in the quadratic constraint (5) [7, 8]. That matrix has exactly one positive and two negative eigenvalues. As a result, according to the inference in §2.3, a single ellipse is selected by requesting  $c=1$ , while two hyperbolas are very likely to be selected by requesting  $c=-1$ . As for parabolas, they correspond to the singularities of such a scaling, and are thus avoided. As a side effect, the shape of the fitted ellipse and hyperbolas is biased towards lower and higher eccentricity, respectively.

The extension of this previous approach to the 3D case of quadratic surfaces is not straightforward. The main issue is the *third order* of  $\det(\Omega)$ : enforcing  $\det(\Omega)=+1$  for instance falls outside the framework of closed-form least squares. In addition, in the 3D case the sign of  $\det(\Omega)$  gets changed according to the unknown orientation of the quadric normals (see §3.2). For instance,  $\det(\Omega)$  is positive both for an outward-pointing E and for an inward-pointing H1 (Fig.1). Moreover, if further discrimination is needed between types, for instance between H1 and H2, the quartic  $\det(\Omega^h)$  must also become involved somehow, whereas this is not an issue for ellipsoid guaranteeing.

First solving the problem subject to only one constraint and testing afterwards if the output meets the second constraint, as performed in [11] for ellipsoid fitting, cannot provide the user with a guarantee. To keep to the framework of robust closed-form eigenvalue resolution as in §2, we need to stick to a *single* type-guaranteeing *quadratic* constraint, like in [13] in the case of ellipsoid specificity. We now describe a way to follow such a track.

#### 4.1. Exploring enforceable constraints on quadrics

In this work, we intentionally investigate *all* possibilities of enforceable quadratic constraints. To this end, we have logically devised a combination of the first two symmetric invariants (11), by introducing the two scalars  $\alpha$  and  $\eta$ :

$$\begin{aligned} c_{\alpha,\eta}(\Omega) &= \alpha \sum \det^p_2(\Omega) + \eta \operatorname{tr}(\Omega)^2 \\ &= \alpha_1^2 (\eta \beta^2 + \eta \gamma^2 + (\alpha-2)(\beta\gamma + \gamma + \beta) + \eta). \end{aligned} \quad (14)$$

Thus, for  $\eta = -1$ , this turns into the quantity considered in [13]. In order to explore exhaustively the entire research space, one actually just needs to consider: –this non-zero case when  $\eta = -1$ , while having the parameter  $\alpha$  vary; –in addition, the zero case  $\eta = 0$  with for instance  $\alpha = +1$ . For simplicity we shall further denote them  $c_\alpha(\Omega)$  and  $c_{+\alpha}(\Omega)$ .

We have observed that the sign of the quantity  $c_\alpha(\Omega)$  (14) depends on the coordinates  $\beta$  and  $\gamma$  through an affine quadratic form of known coefficients. In particular, its zero-set  $Z_\alpha$  is a conic curve in the QSM, which we have geometrically characterized and plotted in Fig.2, according to the numerical value of parameter  $\alpha$ . As can be noticed, every conic  $Z_\alpha$  is diagonally aligned. As for its 2D conic type, we report, as can be followed in Fig.2, that:

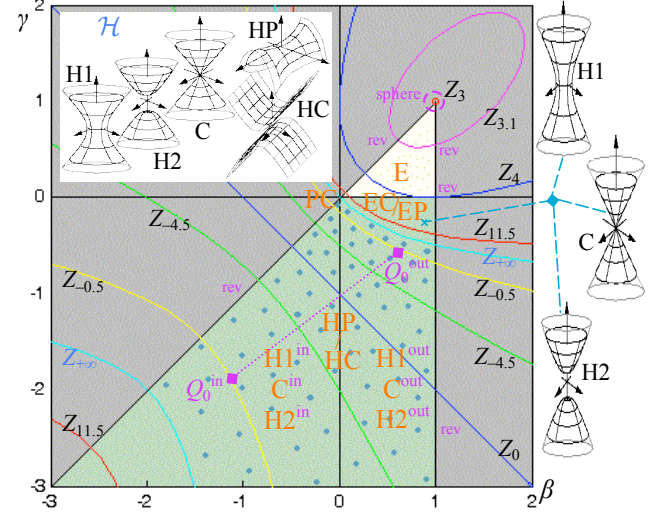


Figure 2: The zero-set  $Z_\alpha$  of constrainable quadratic  $c_\alpha(\Omega)$  (14), plotted for several significant values of parameter  $\alpha$  (§4.1) in the QSM;  $Z_{+\alpha}$  encloses the blue-dotted region, yielding a constraint

- when  $\alpha < 0$ ,  $Z_\alpha$  is an outward-pointing hyperbola;
- for  $\alpha = 0$ ,  $Z_\alpha$  is a pair of coincident lines (coincident with the kernel of the trace in Fig.1.i);
- when  $\alpha > 0$ ,  $Z_\alpha$  is inward-pointing. Moreover, as  $\alpha$  goes on further increasing, its shape evolves in the QSM:
  - $Z_\alpha$  is an imaginary ellipse when  $\alpha < 3$  (since  $c_2$  is always negative, non-specific constraint  $c_2(\Omega) = -3$  can be used as the normalization factor [3, 6, 2]);
  - $Z_\alpha$  appears in the QSM as single point (1,1) for  $\alpha = 3$ ,
  - then grows as a real ellipse enclosing (1,1) when  $\alpha > 3$ ,
  - which opens into a parabola for  $\alpha = 4$ ;
  - then, when  $\alpha > 4$ ,  $Z_\alpha$  becomes a hyperbola, which tends to be the rectangular  $Z_{+\infty}$  as  $\alpha$  further increases towards  $+\infty$  (getting close to the curve in Fig.1.ii).

Now, in the QSM in Fig.2, we can determine whether a given quadric  $Q_0$  satisfies a constraint on the sign of  $c_\alpha(\Omega_0)$  by checking whether the associated point  $(\beta_0, \gamma_0)$  is inside or outside the oriented curve  $Z_\alpha$ . One can now observe that, in this parameterized curve network, the *only* curves  $Z_\alpha$  that can enclose a region within a type-characteristic zone in the QSM are those for  $3 \leq \alpha \leq 4$ , which we have reported in [13] thus shedding a new light on the condition proposed in [12]. Best with  $\alpha = 4$ , this leads to a sufficient condition guaranteeing *at least* one output ellipsoid E, which is yet limited since flat-shaped ellipsoids are out of guarantee, and restrictive due to the singularities associated with the points along  $Z_4$  [13]. We have used this constraint to help characterize the complex wrist joint.

#### 4.2. A new constraint to study saddle-like shapes

Now, at seeking specificity to other types, we have found that another similar constraint is enforceable. There is no other contour enclosing a *single* characteristic zone;

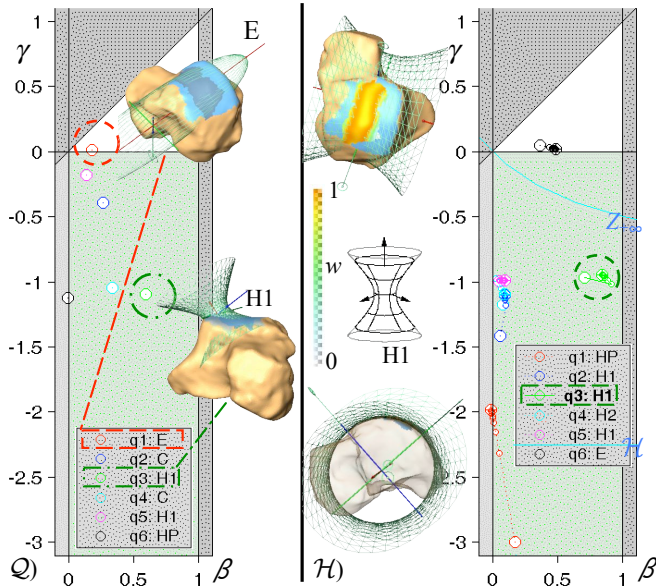


Figure 3: Characterization of the trochlea groove of a problematic talus bone (ankle), both in 3D space and in the QSM [2]:  $-\mathcal{Q}$ ) helpless output primitives of direct fitting without topological constraint, featuring a borderline E and an irrelevant H1;  $-\mathcal{H}$ ) relevant H1 fit from enforcing prior-knowledge, further refined through robust IRLS (converging tails in QSM), providing: articular symmetry axes (R/G/B) joining at symmetry center, extremal curvature radii and centers (green pins), final influence weight colorwash map (hue and value are proportional to the fitting goodness at inlying points, outliers are left white)

thus, one can try to enclose *several* characteristic zones. In Fig.1 and Fig.2, it can be noticed that the constraint  $c_{+\infty}(\Omega) < 0$ , that is  $\sum \det^p_2(\Omega) < 0$ , is a *sufficient condition* for the quadric to be of one of the types H1, H2, C, HP, and HC. These are *exactly the types of quadrics that intersect at least one plane in a hyperbola* (let us denote this character ‘ $\mathcal{H}$ ’). Again it is a sufficient condition for the quadric to be among this family, yet *not with any* shape. A subset of hyperboloids is then not included in the guarantee. These are associated with some point located on the non blue-dotted outside of the branches of  $Z_{+\infty}$  in the QSM, e.g. in the right upper corner of the H1/C/H2-zone (then the absolute value of the two positive eigenvalues  $\alpha_1$  and  $\alpha_2$  of  $\Omega$  is relatively high with respect to the one of the negative  $\alpha_3$  associated with the red axis). As for shape, the hyperboloids in this latter particular case (Fig.2) are rather elongated ones (each semi-axis of a quadric is proportional to the square root of the absolute reciprocal of the resp.  $\alpha_i$ ). Meanwhile, all HP and HC are included in the guarantee.

Fig.2 also shows that, as soon as  $\alpha$  is finite, the constraint  $c_\alpha(\Omega) < 0$  no longer guarantees the  $\mathcal{H}$  character since the curve  $Z_\alpha$  then encloses other types of quadrics in the QSM (namely PC, EC, EP, E).

*N.B.* It can be noticed in Fig.2 that the  $\{\beta=0, \gamma < 0\}$  demi-axis splits the lower half-plane of the QSM into the lower left and right quadrant associated with inward-pointing

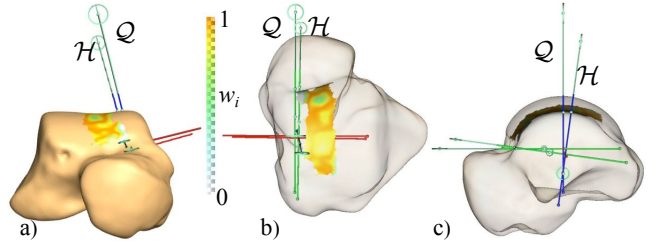


Figure 4: Comparative superimposition of extracted global features with vs. without prior knowledge from an easy talus bone: main orientation and curvature centers actually coincide

and outward-pointing quadric surfaces respectively. Given a point for instance  $(\beta_0^{\text{in}}, \gamma_0^{\text{in}})$  in the lower left-hand quadrant, the coordinates of the *dual* point in the lower right-hand quadrant that is associated with the very same hyperboloid or cone having outward-pointing normals are:  $(\beta_0^{\text{out}}, \gamma_0^{\text{out}}) = (\beta_0^{\text{in}}/\gamma_0^{\text{in}}, 1/\gamma_0^{\text{in}})$ . This sort of coordinate-dependent central dilation formula of center  $(0, -1)$  and negative factor  $1/\gamma_0^{\text{in}}$  holds reciprocally. It can be checked that, when a H1/C/H2 meets the symmetric quadratic constraint, so does its oppositely oriented dual in the QSM.

In the practical estimation, the chosen constraint  $\sum \det^p_2(\Omega) < 0$  is merged with the normalization constraint in the quadratic constraint (5) by setting  $c = -1$  and enforcing the equality constraint:

$$\sum \det^p_2(\Omega) = -1. \quad (15)$$

The  $6 \times 6$  nonsingular constraint submatrix involved in the quadratic constraint (5) is then ( $\mathbf{I}_3$  the  $3 \times 3$  identity matrix):

$$\mathbf{C}_q = \begin{pmatrix} 0 & \frac{1}{2} & \frac{1}{2} & & & \\ \frac{1}{2} & 0 & \frac{1}{2} & & & \\ \frac{1}{2} & \frac{1}{2} & 0 & & & \\ & & & \mathbf{0}_{3 \times 3} & & \\ & & & & -\frac{1}{4} \mathbf{I}_3 & \end{pmatrix}. \quad (16)$$

This matrix has 2 multiple negative and 1 simple positive eigenvalues. As can be inferred from Sylvester’s Law of inertia and Fig.2, the specificity-enforcing constraint is satisfied by the 5 eigenvectors associated with either negative eigenvalue of  $\mathbf{C}_q$  (satisfying  $c_\alpha(\Omega) = -1$ ), and ensures that these yield solutions from among H1, H2, C, HP, HC. Meanwhile, no guarantee is given about the type of the quadric implied by the sixth output parameter eigenvector of (7) that meets the opposite constraint  $c_\alpha(\Omega) = +1$ . Nearly any quadric might be output, save HP, HC and PC: say E, PE, CE or even elongated H1 / C / H2. As a matter of fact, this method thus yields *at least five* primitives with  $\mathcal{H}$  character. If an elongated hyperboloid is to definitely suit the input data, then it is probable –yet not guaranteed– that it will be output, associated with a point on the outside of  $Z_{+\infty}$ . In this case, it may still be interactively selected by the operator among the output eigendecomposition.

In addition, the shape of the guaranteed  $\mathcal{H}$ -type quadrics (and of all fitted primitives) tends to qualitatively keep away from the shape of all the repulsive singularities of the implied normalization equality constraint ( $|\sum \det^p_2(\Omega)| = 1$ )

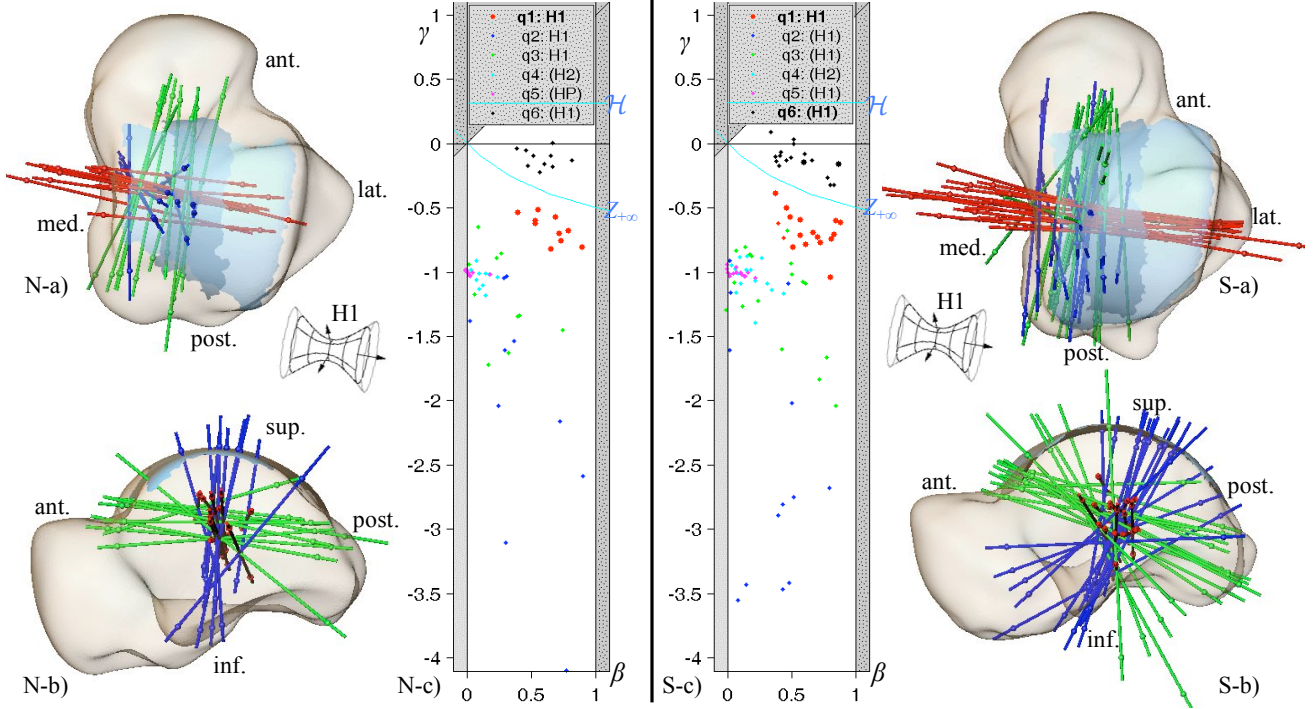


Figure 5: Prior-knowledge-driven comparative characterization of the trochlea groove in the database of all 10 talus samples of Homo Neanderthalensis (N) and all 17 talus samples of Homo Sapiens (S): extracted intrinsic symmetry-axis 3D frames superimposed in superior and medial views (a & b); accumulated eigendecompositions in the QSM, providing consistent mensuration signatures (c)

which are associated with points along the curve  $Z_{+\infty}$ . For instance, the outputs avoid resembling parabolic cylinders PC (associated with the origin in the QSM), as well as all the rather elongated hyperboloids and cones that are associated with every point  $(1/m, -1/(m+1))$  and its dual, where  $m$  is a positive integer, including the very ones of revolution associated with point  $(1, -1/2)$  in the QSM (or its dual  $(-2, -2)$  alike). Also, primitives associated with points in the vicinity of the former points are difficult to fit in practice. The output hyperboloids are to be finally less elongated than the point cloud data actually looks like.

## 5. Application to an ankle database

This new type-guaranteeing constraint (15) that we have introduced happens to be especially suitable to guide the characterization of articular surfaces that are convex along one direction and concave along another: for instance, trochleae involved in the three human hinge (gynglimus) joints –via expectable types H1 or  $C_-$ , or surfaces involved in the three human saddle joints achieving a universal joint biomechanical liaison (via type PH). The trochlear articular surface of the talus bone is involved in the 1-degree-of-freedom flexion–extension motion of the ankle joint, which orients the foot in a nearly sagittal plane. It is highly convex in this plane, while being slightly concave transversally. We here characterize the ‘V’ groove part of its usually smoothed ‘ $\Sigma$ ’ profile. Features of interest to be extracted with respect to the trochlea are: –the plane of its groove and the

corresponding rotation axis; –its angular extent and longitudinal curvature; –the re-questioned circularity and locations of extremal curvature.

We have applied this type-enforceable scheme to an available database of anthropological talus bone samples: 10 from Homo Neanderthalensis, 17 from medieval Homo Sapiens. Note the high variability of the talus, already among modern human beings, yet to be quantified. The dry bone samples were digitized with CT, segmented, scaled to a normalized volume, and initially aligned based on inertia axes. As a dual step upstream of our characterization, the groove surface of the talocrural trochlea was then selected semi-interactively within the talus surface, based on the local Gaussian curvature hierarchized information [15]. We have processed the resulting point cloud data only.

Essentially because of the bad conservation of certain samples, prior knowledge has proved needed since generic fits fail to ensure a stable realistic axis extraction (Fig.3,  $Q$  vs.  $\mathcal{H}$ ). The *a priori* knowledge is about the morpho-functional class as a hinge joint. In this case a reliable characterization is provided by a H1 fit, helped or not. Our target is the *repeatability* of a pertinent and comparable characterization from one sample to the next. Thus we coherently apply the same type-guaranteed fitting, even to easy the samples that could have been characterized without prior knowledge. As a consequence, for these cases we need to assess the *bias* implied by over-imposing the  $\mathcal{H}$ -type prior compared with pure generic ( $Q$ ) fitting,

as exemplified in Fig. 4. So far, only a slight difference of orientation in coincident near-sagittal planes is observed, and the extremal curvature centers do coincide. The results of the homogeneous processing of the whole database offer a differentiation between the two species (Fig.5). It is remarkable to see: a) the pose consistency of the intrinsic frames; b) the coherent clusters appearing as true comparable *signatures* in the QSM. Besides, the absence of points near boundaries refutes the usually expected circularity in the longitudinal plane of the trochlea: e.g. curvature radii are shorter along anteroposterior axis than vertically (cf. Fig.4.c). In fact, as shown by the orientation of the blue and green axes, whereas for *Homo Neanderthalensis* the curvature level is balanced from back to front in the near-sagittal intrinsic global-symmetry plane (Fig.5.N.b), the anterior portion (ant.) of the groove of the *Homo Sapiens talus trochlea* is more curved than its posterior part (post. Fig.5.S.b). This confirms kinematical results of a recent biomechanical study which performed passive motion of half a dozen of specimen ankle from modern humans [16].

Aside from such an anthropologic challenge of inferring the gait motion and standing posture from the analysis of shape only –sometimes poorly conserved–, this method is also of high clinical relevance, especially providing centers and axes for prosthetics pose and design. The implemented tool is ready to be used without modification to carry out the study of some *in vivo* database, which promises to be interesting on healthy and pathological talus bones. This can be applied on point clouds stemming from noisy preprocessed volumetric images, but also from exposed joint palpation. Furthermore, if kinematic information is available in terms of helical axes, the extracted intrinsic frame here is to be a privileged viewpoint for its display.

## 6. Discussion and perspectives

In this feasibility study we have utilized the Quadric Shape Map as a convenient 2D diagram to explore, devise and study enforceable type-guaranteeing constraints when fitting quadrics to point data. As a result, we propose one new quadratic constraint that enforces outputs to be among the hyperbolic-section ‘ $\mathcal{H}$ ’ family, including hyperboloids. It comes in addition to the available ellipsoid-guaranteeing constraint. It is less exclusive, being specific to a group of types of quadrics, without more precision. However, in practice, a relevant primitive of the expected type has so far always occurred in the output eigendecomposition. The only ambiguity we have encountered is outputs of type H1 instead of HP at the thumb, both being saddle-like types. This tool might be used for other applications to help retrieve H2/HC types. A more critical issue is the limitedness or even restrictiveness of the guaranteeing constraints against certain mensurations, due to the set of singularities crossing through the QSM research space. This should be experimentally assessed on natural and corrupted data.

Unified closed-form linearity is a methodological feature that we have valued so far and, as we have proved, the framework is then limiting as regards possibilities of typological constraints. Sharper enforcement of separate types (including cones and cylinders) remains in prospect. We also intend to focus on the refinement of the robust norm. In a way, as it is, some localized discriminating information is additionally conveyed via the point weights distributed by the M-estimator. Handling this information by patches of points instead of individually is likely to help significantly the eigenprimitive extraction within poorly segmented or pathological structures. It may further reveal *shape as a print of function and as a footprint of evolution*.

## References

- [1] J. Hohe, G.A. Ateshian, M. Reiser, K.-H. Englmeier, F. Eckstein. Surface size, curvature analysis, and assessment of knee joint incongruity with MR imaging in vivo. *Magnetic Resonance in Med.*, 47(3):554–561, Mar. 2002.
- [2] S. Allaire, *et al.* Robust Quadric Fitting and Mensuration Comparison in a Mapping Space Applied to 3D Morphological Characterization of Articular Surfaces. In *proc. of the 4<sup>th</sup> IEEE ISBI*, 972–975, Apr. 2007.
- [3] F.L. Bookstein. Fitting Conic Sections to Scattered Data. *Comp. Graph. and Image Proc.*, 9(1):56–71, Jan. 1979.
- [4] P.D. Sampson. Fitting Conic Sections to "Very Scattered" Data: An Iterative Refinement of the Bookstein Algorithm. *Comput. Graph. Image Proc.*, 18(1):97–108, Jan. 1982.
- [5] P.L. Rosin. A note on the least squares fitting of ellipses. *Pattern Recognition Letters*, 14(10):799–808, Oct. 1993.
- [6] W. Gander, G.H. Golub, R. Strebel. Least-Squares Fitting of Circles and Ellipses. *BIT*, 34:558–578, 1994.
- [7] A.W. Fitzgibbon, M. Pilu, R.B. Fisher. Direct Least Square Fitting of Ellipses. *IEEE T PAMI*, 21(5):476–480, 1999.
- [8] R. Halif. Robust bias-corrected least squares fitting of ellipses. In *proceedings of WSCG, vol. I-II*, Feb. 2000.
- [9] N. Werghi, R.B. Fisher, C. Robertson, and A.P. Ashbrook. Modelling Objects Having Quadric Surfaces Incorporating Geometric Constraints. In *proc. ECCV*, 2:185–201, 1998.
- [10] S.J. Ahn, W. Rauh, H.S. Cho, and H.J. Warnecke. Orthogonal Distance Fitting of Implicit Curves and Surfaces. *IEEE T PAMI*, 24(5):620–638, May 2002.
- [11] N. Grammalidis, N. Sarris, C. Varzokas, and M.G. Strintzis. Generation of 3-D Head Models from Multiple Images Using Ellipsoid Approximation for the Rear Part. In *proceedings of the 7th IEEE ICIP*, 1:284–287, Sept. 2000.
- [12] Q. Li and J.G. Griffiths. Least Squares Ellipsoid Specific Fitting. In *proc. of the IEEE CS GMP*, 335–340, Apr. 2004.
- [13] S. Allaire, J.-J. Jacq, V. Burdin, Ch. Roux. Ellipsoid-Constrained Robust Fitting of Quadrics with Application to the 3D Morphological Characterization of Articular Surfaces. In *proc. of the 29<sup>th</sup> IEEE EMBC*, Aug. 2007.
- [14] W.H. Beyer. *Standard Mathematical Tables*, CRC, 1978.
- [15] J.-J. Jacq, C. Roux. Geodesic Morphometry with Applications to 3D Morpho-Functional Anatomy. *Proceedings of the IEEE*, 91(10):1680–1698, Oct. 2003.
- [16] A. Leardini, J. J. O’Connor, F. Catani, S. Giannini. A geometric model of the human ankle joint. *Journal of Biomechanics*, 32:585–591, 1999